Geophysical Research Letters

RESEARCH LETTER
10.1029/2022GL098571

Teleconnection Patterns of Different El Niño Types Revealed by Climate Network Curvature

Felix M. Strnad[1], Jakob Schlör[1], Christian Fröhlich[1], and Bedartha Goswami[1]

[1]Cluster of Excellence Machine Learning: New Perspectives for Science, Universität Tübingen, Tübingen, Germany

Felix M. Strnad and Jakob Schlör contributed equally to this work.

Key Points:

- Ricci curvature of boreal winter climate networks reveals long-range teleconnection structure
- Eastern Pacific (EP) El Niños show primarily teleconnections in tropical while Central Pacific El Niños teleconnections on all latitudes
- The EP contains robust teleconnections for both El Niño types

Supporting Information:

Supporting Information may be found in the online version of this article.

Correspondence to:

F. M. Strnad and J. Schlör,
felix.strnad@uni-tuebingen.de;
jakob.schloer@uni-tuebingen.de

Citation:

Strnad, F. M., Schlör, J., Fröhlich, C., & Goswami, B. (2022). Teleconnection patterns of different El Niño types revealed by climate network curvature. *Geophysical Research Letters*, *49*, e2022GL098571. https://doi.org/10.1029/2022GL098571

Received 4 MAR 2022
Accepted 24 AUG 2022

Author Contributions:

Conceptualization: Felix M. Strnad, Jakob Schlör, Bedartha Goswami
Formal analysis: Felix M. Strnad, Jakob Schlör, Bedartha Goswami
Investigation: Felix M. Strnad, Jakob Schlör, Christian Fröhlich, Bedartha Goswami
Methodology: Felix M. Strnad, Jakob Schlör, Christian Fröhlich
Software: Felix M. Strnad, Jakob Schlör, Bedartha Goswami
Supervision: Bedartha Goswami
Validation: Felix M. Strnad, Jakob Schlör, Bedartha Goswami

Abstract The diversity of El Niño events is commonly described by two distinct flavors, the Eastern Pacific (EP) and Central Pacific (CP) type. While the remote impacts, that is, teleconnections, of EP and CP events have been studied for different regions individually, a global picture of their structure is still lacking. Here, we use Forman-Ricci curvature applied on climate networks constructed from surface air temperature data to distinguish regional links from teleconnections. Our results confirm that both El Niño types influence the teleconnection patterns, however, with different spatial manifestations. Our analysis suggests that EP El Niños alter the general circulation which changes the teleconnection structure to primarily tropical teleconnections. In contrast, the teleconnection pattern of CP El Niños show only subtle changes to normal conditions. Moreover, this work identifies the dynamics of the Eastern Pacific as a proxy for the remote impact of both El Niño types.

Plain Language Summary El Niño events, characterized by anomalous sea surface temperatures (SSTs) in the Tropical Pacific, come in two flavors; Eastern Pacific (EP) and Central Pacific (CP) types, depending on the longitudinal location of the strongest SST anomalies. Their remote impacts, known as teleconnections, differ. Although there are many studies investigating teleconnections of EP and CP events for individual target regions, a global analysis of the spatial distribution of their teleconnections is still lacking. In this study, we use the theory of complex networks to study EP and CP El Niño teleconnections. We construct "climate networks" from global surface air temperature data and use the notion of "curvature" of a network link to uncover their spatial organization. We show that the most negatively curved links highlight important teleconnection patterns that differ depending on the El Niño type. EP events change the teleconnection structure to the tropics while CP and Normal year conditions reveal teleconnections to all latitudes. Interestingly, the Central Pacific does not show many teleconnections, even during CP El Niño events which we attribute to the varying location of warm water anomalies in the Central Pacific. The Eastern Pacific changes more consistently allowing identifying remote impacts of both El Niños types.

1. Introduction

The El Niño-Southern Oscillation (ENSO) is the most dominant interannual variation in the global climate system. It is a dynamical atmospheric and oceanic phenomenon characterized by anomalously warm (El Niño) or cold (La Niña) phases of sea surface temperatures (SSTs) in the Equatorial Pacific. Both phases are known to impact Earth's climate significantly on large spatial scales, typically referred to as teleconnections (Trenberth, 1997) and thus have been investigated in many studies over the past two decades (Capotondi et al., 2015, 2020; Timmermann et al., 2018).

Yet, significant differences in the downstream impacts of El Niño events are reported (Shi et al., 2019), depending on the amplitude and spatial position of SST anomalies. These differences can be partly related to the type of El Niño. The diversity of El Niño events is typically characterized by two modes: The "canonical" or Eastern Pacific (EP) El Niño (Rasmusson & Carpenter, 1982) with peak SST anomalies in the eastern equatorial Pacific, and the "El Niño Modoki" (Ashok et al., 2007) or Central Pacific (CP) El Niño with peak SST anomalies in the Central Equatorial Pacific (Kao & Yu, 2009). Although the effect of both El Niño types on different locations of the Earth—such as the Indian Ocean (IO) (e.g., Klein et al., 1999), maritime continent (e.g., G. Wang and Hendon 2007), tropical Atlantic (e.g., Huang 2004), and Northern America (e.g., Yu et al., 2012)—has been studied thoroughly (see Okumura 2019 and Taschetto et al., 2020 for an overview), previous work has mainly focused on single teleconnections of the El Niño types.

In comparison, little is known about differences in the spatial extent of global teleconnection patterns between EP and CP events. In this study, we address this issue by introducing a novel machine learning approach that

Visualization: Felix M. Strnad, Jakob Schlör
Writing – original draft: Felix M. Strnad, Jakob Schlör
Writing – review & editing: Felix M. Strnad, Jakob Schlör, Christian Fröhlich, Bedartha Goswami

employs climate networks combined with Ricci-curvature, an abstract tool from the theory of complex networks. Climate networks (Dijkstra et al., 2019) have gained increasing interest in the analysis of spatial dependencies of climatic variables through their ability to reduce data to relevant climatic patterns, and therefore, have been widely used in the analysis of ENSO. Tsonis and Swanson (2008) investigated the topology of El Niño and La Niña networks of surface air temperature. The global impact of El Niño on various geographical zones (Yamasaki et al., 2008), on geographical long-range teleconnections (Donges et al., 2009; Zhou et al., 2015), and its diversity (Kittel et al., 2021; Radebach et al., 2013) have been analyzed by evolving climate network analyses. Wiedermann et al. (2016) employ them to find a robust way to distinguish between different types of El Niños flavors and Lu et al. (2020) estimate the expected El Niño impacts by using climate networks. Ricci-curvature of complex networks is a recent approach to visualize the structure of a network intuitively by highlighting whether an edge of the network connects nodes within a community (i.e., a group of densely connected nodes) or bridges two communities (Ollivier, 2009; Sreejith et al., 2016). It has been proven useful, for example, in the analysis of financial markets (R. S. Sandhu et al., 2016), gene expressions (Pouryahya et al., 2018; R. Sandhu et al., 2015), brain connectivity (Farooq et al., 2019), urban transportation (Gao et al., 2019), power grids (Jonckheere & Grippo, 2019), and epidemiology (de Souza et al., 2021). We show that our approach is an intuitive yet informative tool to analyze the spatial organization of teleconnections that outlines structural differences between EP and CP El Niño impacts.

2. Data and Methods

2.1. Data

We use daily surface air temperature (SAT, 2-m air temperature) data for the years 1959–2020 from the ERA5 Global Reanalysis database (Hersbach et al., 2020). We first detrend each time series, then subtract the daily climatology of the whole time period resulting in anomaly time series with respect to the day of the year. We use next-neighbor interpolation to map the data to a grid of spatially approximately uniformly distributed points using the Fekete algorithm (Bendito et al., 2007) to avoid spurious correlation patterns close to the poles (Ebert-Uphoff & Deng, 2012) (see Section 4.1 and Figure S5 in Supporting Information S1). The distance between grid points in the Fekete grid corresponds to the distance between two points at the equator of a 2.5° Gaussian grid, resulting in a total of ≈6,000 grid points.

2.2. Classification of EP and CP El Niño Conditions

We use December–February daily SAT anomalies and select EP El Niño, CP El Niño, and "Normal" winters based on the average DJF SST anomalies in the Niño 3 (N3) and Niño 4 (N4) region (Trenberth & Stepaniak, 2001). We classify a winter as EP (CP) event if N3 is greater (less) than N4 and N3 (N4) larger than 0.5 (Capotondi et al., 2020). Winters with N3 and N4 between −0.5 and 0.5 are labeled as "Normal". The SST anomalies are calculated using a centered sliding-window 30-year base period, successively updated in 5-year steps (see Section 1 and Table S1 in Supporting Information S1). Although the onset and duration of El Niño events show high variability, we restrict our analysis to the December–February period where El Niño events show in general the highest intensities to avoid seasonality effects in our analysis.

2.3. Ricci Curvature of Correlation-Based Climate Networks

We demonstrate the process of computing the curvature of a climate network using a toy data set. Figure 1a denotes a set of time series distributed over a sphere. Correlations between all pairs of time series are *predefined* (in contrast to our actual SAT data set) with a priori fixed covariance structure created from a stochastic block model (see Section 2 in Supporting Information S1). In order to calculate the Ricci curvature, we first need to create a climate network, which signifies the most related grid points over the entire globe. The network is determined by considering the 2% strongest ($\rho_{0.98}$) statistically significant correlations ρ_{ij} between pairs of time series $x_i(t)$, $x_j(t)$ which is described by the weighted adjacency matrix $\mathbf{W}_{ij}$ (Figure 1b):

$$\mathbf{W}_{ij} = \begin{cases} |\rho_{ij}|, & |\rho_{ij}| > \rho_{0.98}, \\ 0, & \text{otherwise}. \end{cases} \tag{1}$$

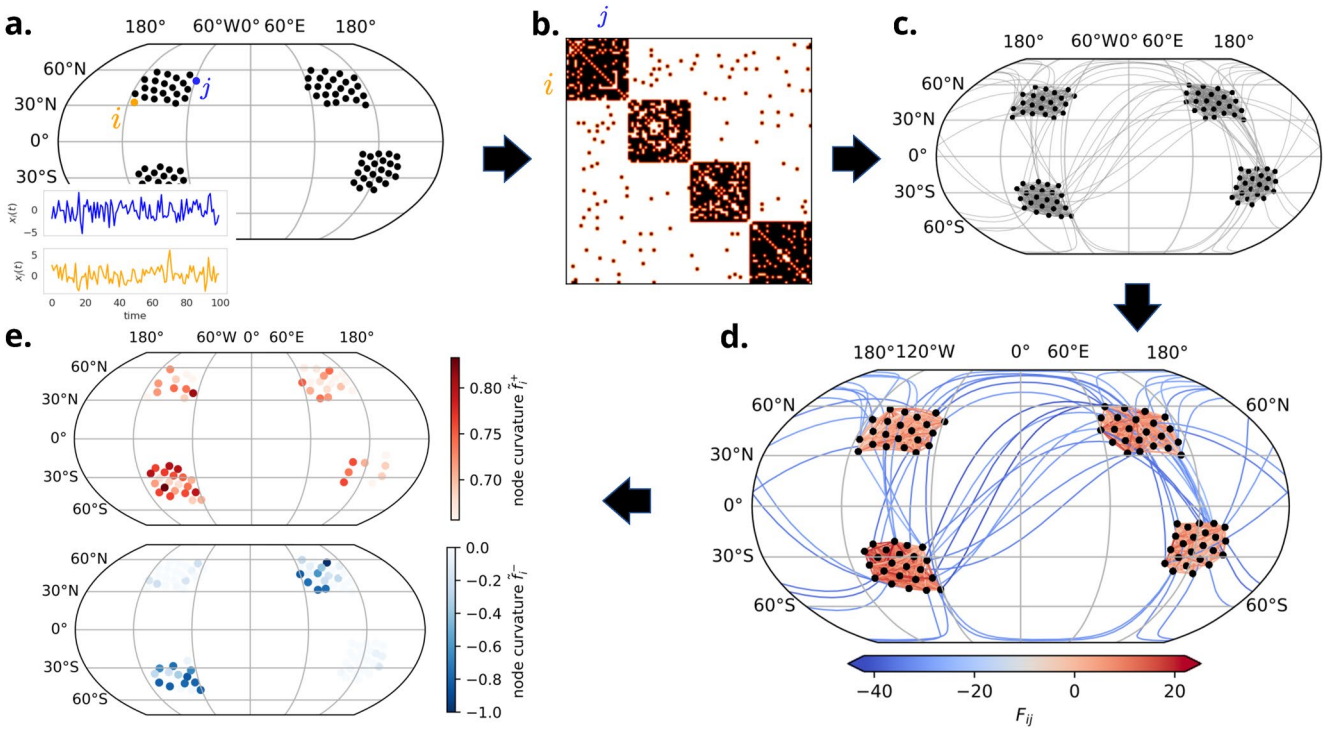

Figure 1. Construction of a climate network and its curvature measure for a toy data set. By computing correlations of time series between all pairs of locations (a), we obtain the adjacency matrix $\mathbf{W}_{ij}$ (Equation 1), orange dots denote points of significant correlations between time series $x_i(t)$, $x_j(t)$ (b), visualized as a network graph (c). The Forman curvature F_{ij} of each edge (d) reveals the property of an edge as within-community (positive curvature) or bridging communities (negative curvature). Positive (negative) node curvature hotspots f_{ij}^+ $\left(f_{ij}^-\right)$ (e) are obtained by aggregating the 10% most positively and 10% most negatively curved edges on the nodes.

This is equivalent to a network G whose nodes $V = \{v_i: i = 1, .., N\}$ correspond to spatial locations $i = 1, \ldots, N$ with edge e_{ij} connecting the nodes $(v_i, v_j) \in V$ if $|\rho_{ij}| > \rho_{0.98}$ (Figure 1c) weighted by ρ_{ij} (for details see Section 3.2 in Supporting Information S1).

Ricci curvature provides a continuous measure over network links (i.e., independent from the spatial grid) using the connectivity between points to describe their relationship in the network. Figure 1d shows the network of our toy example with their edges e_{ij} colored by their curvature F_{ij}.

We see that positive curvature indicates an edge being embedded within a community of nodes. The neighborhood of a positively curved edge is more densely connected than a regular graph which is a network with each node containing the same number of neighboring nodes. Positive curvature thus indicates a community of nodes with similar dynamics. Negative curvature corresponds to an edge connecting two communities, with its own neighborhood containing fewer connections than a regular graph. It thus can indicate teleconnections as shown in Section 3.1.

Since multiple edges are difficult to visualize ($\approx 10^6$ links for the SAT network), we define node curvature f_i of the node v_i as the summation of the edge-based measure F_{ij} of all edges e_{ij} connected to v_i. The node curvature is easier to visualize on a map and allows to identify geographical locations connected to strongly negatively or positively curved links. More precisely, we define the upper 90th (lower 10th) percentile of all edges as F_{ij}^+ $\left(F_{ij}^-\right)$ and analogously, and the aggregation of the upper 90th (lower 10th) percentile of the curvature values as f_i^+ $\left(f_i^-\right)$, which we denote as "hotspots" (Figure 1e). As the value ranges differ between networks, we normalize them by using the min-max transformation to $(-1, 1)$, denoted by $\tilde{F}_{ij}$ and analogously, $\tilde{f}_i$ (Equation 9 in Supporting Information S1). The intensity of the positive node-curvature hotspots $\tilde{f}_i^+$ reveals the communities with the highest edge probabilities in the stochastic block model outlining a community of nodes that behave similarly in time. Negative node-curvature hotspots $\tilde{f}_i^-$ coincide with the underlying probabilities used for constructing the data set indicating locations that are highly teleconnected on the globe.

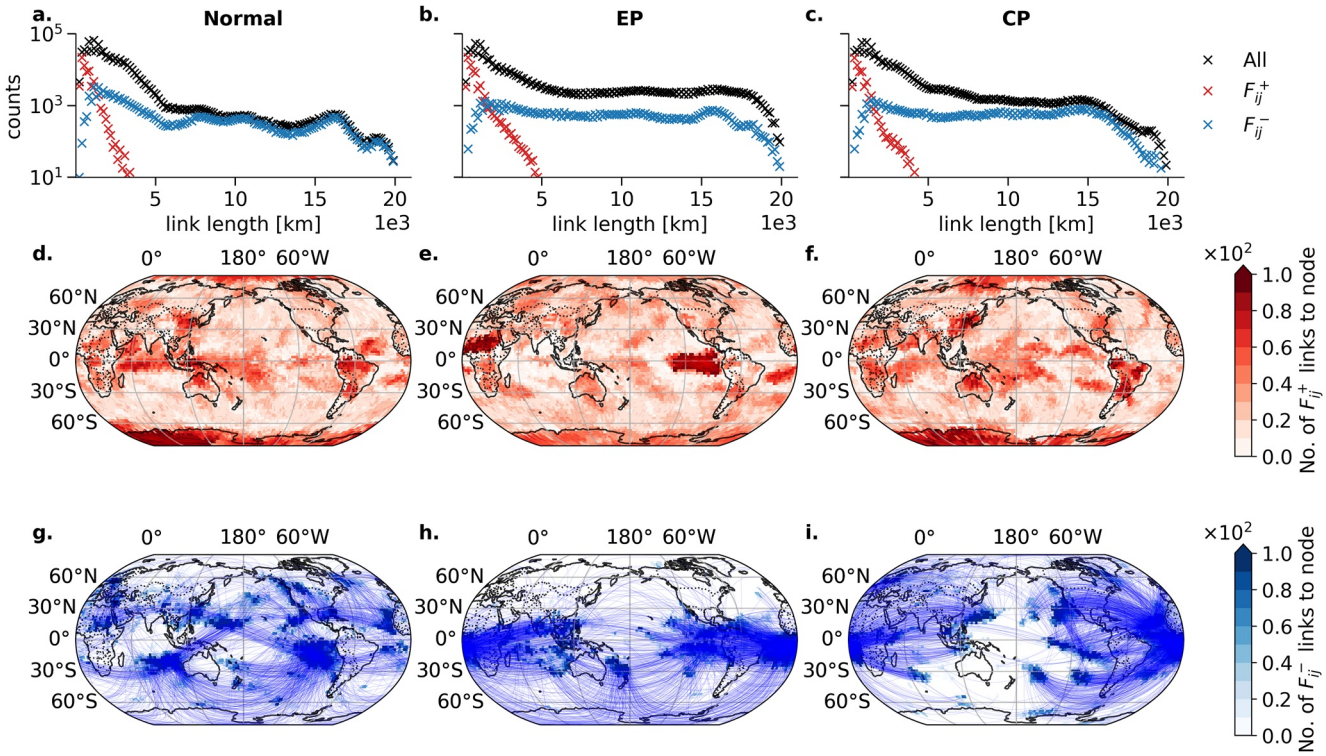

Figure 2. Forman curvature of Normal, Eastern Pacific (EP), and Central Pacific (CP) El Niño climate network links. The networks are computed from surface air temperature (SAT) anomalies for Normal (left column), EP (middle column), and CP (right column) conditions. The first row (a–c) depicts the spatial link length distribution for all (black), most positively F_{ij}^+ (red) and most negatively curved F_{ij}^- (blue) edges. The second row shows F_{ij}^+ (d–f), the third row F_{ij}^- (g–i). Colorbars indicate the number of incoming edges to a node. For visual reasons only every 20th edge is plotted in (d–i).

Of the two numerical approximations of Ricci curvature on networks—Forman-Ricci curvature (Forman, 2003; Sreejith et al., 2016) and Ollivier-Ricci curvature (Ollivier, 2010)—we use Forman-Ricci curvature (henceforth simply Forman curvature) as it is computationally cheaper. Both definitions are highly correlated, barring slight differences in extreme values (Samal et al., 2018). For details on the mathematical description of the curvature method, we refer to Section 4 in Supporting Information S1.

3. Results and Discussion

3.1. Spatial Organization of Teleconnections Depends on El Niño Type

We compute correlation-based climate networks and their Forman curvature using global SAT data for EP, CP, and Normal conditions. Figures 2a–2c show the distribution of spatial link lengths as the shortest distance between two connected points on the globe, the so-called great-circle lengths. Shown are all links of the network (black markers), the most positively curved F_{ij}^+ (red) and most negatively curved F_{ij}^- (blue) network links for Normal, EP, and CP conditions.

The spatial distribution of F_{ij}^+ (Figures 2d–2f) shows that positive curvature occurs at only regional scales $\lesssim 5 \cdot 10^3$ km, resulting in the enforcement of local community structures. While F_{ij}^- links occur at all spatial scales, for lengths $\geq 10^4$ km, the F_{ij}^- and "All" link distributions almost overlaps for CP and Normal conditions. Long-range teleconnections are here thus modulated predominantly via negatively curved links. As the curvature estimation of climate network links does not include any information on the spatial length, this suggests that the relationship between negative climate network link curvature and long spatial scales is an intrinsic topological property of the SAT dynamics. Therefore, negative curvature results in link bundles that are related to well-known teleconnection patterns which are discussed in Section 3.3.

In contrast to CP and Normal conditions, for EP El Niño conditions the distribution of F_{ij}^{-} does not describe all spatially long-range links (Figure 2b) and the most negative network links undergo a drastic spatial reorganization (compare Figure 2h to Figures 2g and 2i). In particular, we observe that the connection between the Tropical Pacific and the southern Atlantic is strengthened during EP conditions (Figure 2h), while during CP El Niños the Tropical Pacific shows an enhanced connection to the extratropical Pacific as well as to the mid-latitude North Atlantic region (Figure 2i, Section 3.3).

Changes in most positively curved links F_{ij}^{+} are more subtle between Normal (Figures 2d and 2f), CP (Figure 2f) and EP conditions (Figure 2e), such as the weakening of regional correlation structures in the tropical Atlantic (CP conditions) and the strengthening of correlation in the Eastern Pacific and the West African monsoon belt (EP conditions).

Note, we mainly discover teleconnections within the global oceans because correlations are generally higher over oceans than over land due to slower oceanic SAT variability (Lambert et al., 2011).

3.2. EP El Niño Conditions Lead to Enforcement of Teleconnections to the Tropics

The global teleconnection pattern is under EP conditions substantially different when compared to Normal conditions (Figures 2 and 3). We suggest that the differences can be attributed to the intensity of the events. EP events tend to have higher temperature anomalies (Figures S2 and S3 in Supporting Information S1) and more stable warming locations in the tropics than CP events (Figure S4 in Supporting Information S1) leading to a strong chan the global atmospheric circulation which results in the confinement of hotspots around the tropics for both regional links and teleconnections. In contrast, CP conditions show unstable warming locations (Figures S2 and S4 in Supporting Information S1) and a weaker amplitude and thus cannot alter the general circulation. Therefore, Normal and CP networks reveal various similarities resulting in positive and negative curvature hotspots over all latitudes (Figure 3). This is further confirmed by the zonal medians (Figures 3g–3i). We repeat our analysis for strong and moderate El Niño events separately (see Section 1 in Supporting Information S1) and find that the EP curvature results (Figure 3) are mainly dominated by the strong EP El Niños (Figures S16 and S17 in Supporting Information S1). We thus conclude that the differences between EP conditions to CP and Normal conditions are driven by strong EP El Niño events. This corroborates previous works by Lu et al. (2020), Wiedermann et al. (2016) who report a strong localization of climate network links during EP conditions as well.

For EP conditions, positive curvature hotspots $\tilde{f}_i^{+}$ reveal the well-known ENSO tongue (Figure 3b) typically observed in empirical orthogonal function analysis of SST data (Johnson, 2013). We also find pronounced regions of $\tilde{f}_i^{+}$ in the IO and the tropical Atlantic which are known to be affected by strong EP El Niño events (Klein et al., 1999; Rodrigues et al., 2015; X. Wang & Wang, 2014; W. Zhang et al., 2015). Under CP conditions, $\tilde{f}_i^{+}$ is spread over all latitudes and over different regions of the globe (Figure 3c). For instance, we observe a hotspot in the Tropical Pacific similar to the El Niño tongue, which is however shifted toward the dateline and also extended southwards.

Negative node-curvature hotspots, $\tilde{f}_i^{-}$, for EP conditions (Figure 3e) show enhanced teleconnections in the South China Sea, tropical IO, Eastern Tropical Pacific, and the tropical Atlantic. This coincides with a decrease in teleconnections in the extratropical Pacific, southern IO, North Atlantic (near Greenland), and the Southern Ocean. Under CP conditions (Figure 3f), we find negative node curvature hotspots in the extratropics and mid-latitudes similar to $\tilde{f}_i^{+}$. While some similarities between CP and Normal conditions are found (Figures 3d and 3f), for example, at the US-West Coast (Capotondi et al., 2019), in the Northern Tropical Pacific, and in the tropical Atlantic, the major difference can be found over the European continent, the Northern Atlantic, and the Labrador Sea (see as well Figures 2g and 2i).

We repeat our analysis using 1,000 years of pre-industrial run of the UKESM1-0-LL model from the CMIP6 project (Eyring et al., 2016) which shows a comparable variation of SSTA in the Tropical Pacific to observational data (Dieppois et al., 2021). We obtain a localization of positive and negative curvature hotspots to the Tropics under EP conditions and teleconnections to the mid-latitudes under CP conditions (see Figure S14 in Supporting Information S1), similar to our analysis of observational data (Figure 3). The longer time period of

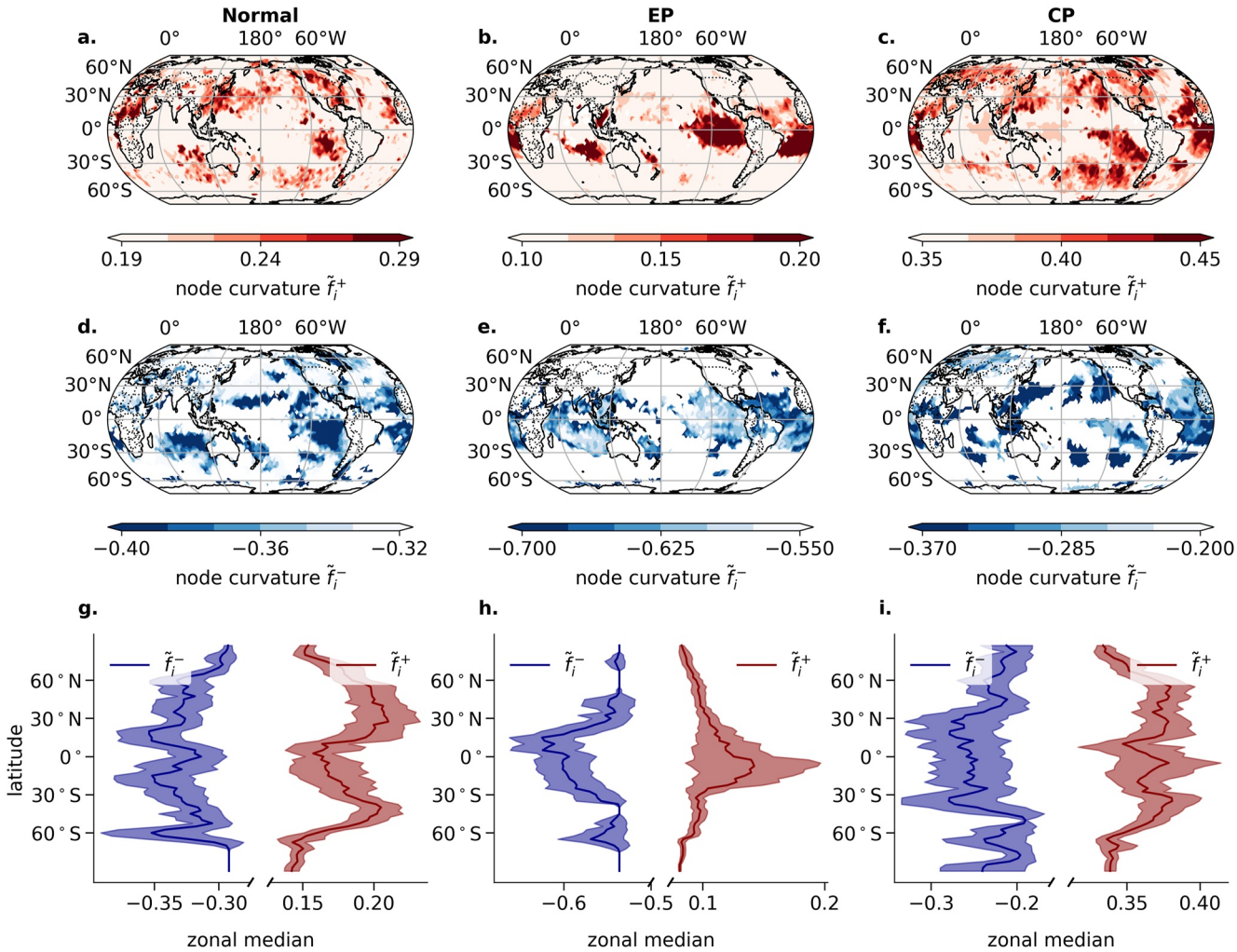

Figure 3. Node curvature of Normal, Eastern Pacific (EP) El Niño, and Central Pacific (CP) El Niño climate networks. Node curvature hotspots for Normal (left column), EP (middle column) CP (right column) hotspots are shown summing the most positively curved $\tilde{f}_i^+$ (a–c), most negatively curved $\tilde{f}_i^-$ (d–f) links, as well as the aggregated zonal medians of $\tilde{f}_i^+$ (red) and $\tilde{f}_i^-$ (blue) (g–i) are shown.

the pre-industrial run allows us to control for the small number of EP and CP events in the reanalysis data set (see Section 7 in Supporting Information S1). We find that the curvature analysis of the reanalysis data with only 7 EP/CP events tend to overestimate the number of negatively curved links. However, qualitatively the spatial patterns of positive and negative curved links are robust in comparison to the 297 EP events obtained in the whole pre-industrial time period (see Figure S15 in Supporting Information S1).

3.3. EP and CP El Niño Teleconnection Patterns of Eastern and Central Pacific Ocean, Indian Ocean, and the Labrador Sea

During EP conditions, teleconnections link the N3 region (Figure 4a) to the tropical Atlantic, supporting earlier work showing that strong El Niños can lead to warming in the tropical Atlantic mediated by the tropospheric temperature mechanism (Chang et al., 2006) and the atmospheric bridge via the Pacific North American (PNA) pattern (Alexander et al., 2002; Rodrigues et al., 2011). The links connecting N3 to the IO are likely apparent because of the influence of Eastern Tropical Pacific SSTs on the IO during and after El Niño events attributed to net heat flux anomalies due to changes in the atmospheric circulation of ENSO (Klein et al., 1999). During CP conditions, we observe links from the N3 box as well, primarily connecting to the extratropical Pacific. These are

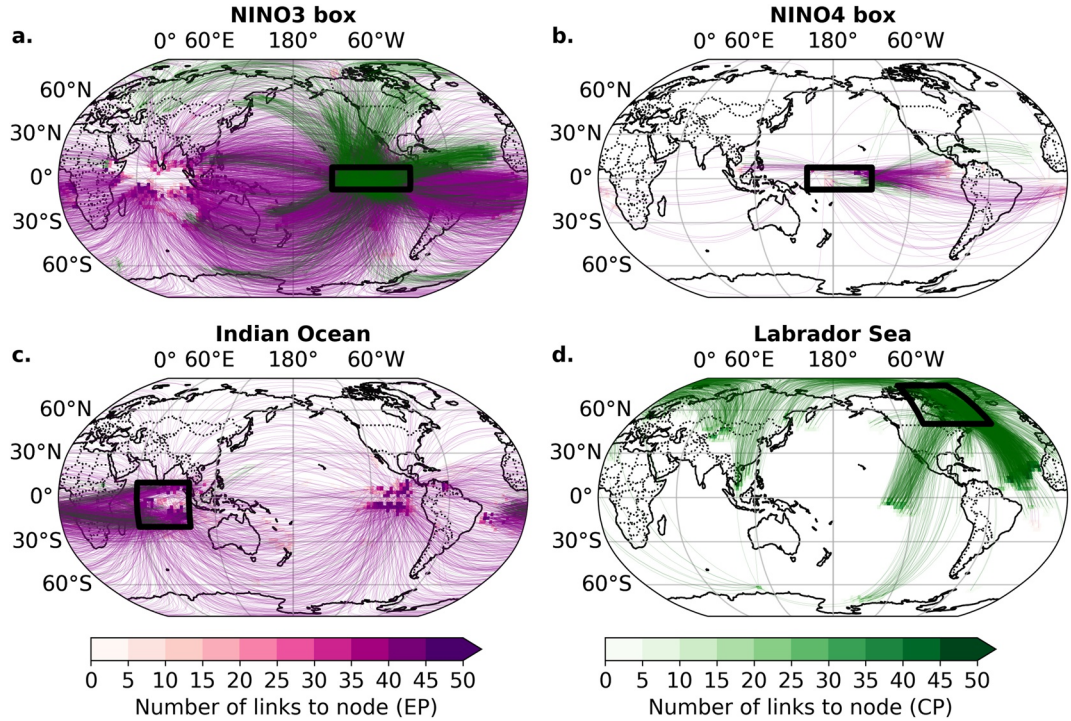

Figure 4. Teleconnections from Eastern and Central Pacific Ocean, Indian Ocean (IO), and the Labrador Sea. F_{ij}^{-}, that is, teleconnections, for EP (purple) and CP (green) El Niño events connected to the four selected regions (black rectangles): Niño 3 (a), Niño 4 (b), IO (c), and Labrador Sea (d). For visual clarity, only a third of all links are shown.

likely due to the North and South Pacific Meridional Mode (NPMM and SPMM), as atmospheric and oceanic anomalies in the extratropics associated with SPMM and NPMM affect the intensity and flavor of El Niño (You & Furtado, 2018). Capotondi and Ricciardulli (2021) showed that the dominant patterns of wind variability in the Northern and Southern Hemispheres, which represent the atmospheric expressions of the NPMM and SPMM, have a stronger relationship with CP events than EP events (Amaya, 2019; Capotondi et al., 2019; Capotondi & Ricciardulli, 2021), consistent with the extratropical links observed during CP events (Figure 4a).

The teleconnections of the N4 region (Figure 4b) are far fewer compared to the N3 region (Figure 4a). It is rather surprising that the N4 region is not well connected even during CP conditions, although a CP El Niño is primarily characterized by higher SST anomalies in the N4 region (Figures S1–S3 in Supporting Information S1). These findings are in apparent disagreement with Barsugli and Sardeshmukh (2002) and Shi et al. (2019) who showed that the PNA and the Northern Pacific are most sensitive to changes of SST in the Central Tropical Pacific using General Circulation Models (GCMs). GCMs are known to produce SST anomalies too far in the west (Capotondi et al., 2006; Ham & Kug, 2012; Kug et al., 2010), however, this can only partially explain the missing teleconnections in the Central Pacific. We find that although anomalies in the Central Pacific are stronger during CP conditions (Figure S1 in Supporting Information S1), the Eastern Pacific shows significantly higher local correlations (Figure S13 in Supporting Information S1). Strong anomalies do not necessarily imply high correlations (compare Section 1 and Figures S2–S4 in Supporting Information S1), therefore, we attribute the weak correlations in the Central Pacific under CP conditions to the higher spatial variability of anomalously warm temperatures between CP El Niño events than between EP El Niño events (Figures S4 and S5 in Supporting Information S1) (Chen et al., 2021; C. Wang & Wang, 2013). During CP conditions, anomalies in the tropical Eastern Pacific are weaker but behave more consistently in time than in the Central Pacific (see Figure S16 in Supporting Information S1). We thus suggest that the teleconnections from the N3 region are artifacts of the correlation but functions as a proxy for the stimulation by the Central Pacific. The results from the curvature analysis using the model output from the UKESM1-0-LL GCM further corroborate our findings. Here as well, N3 teleconnections to the Northern Pacific and west American coast are found in the CP network while the Central Pacific does not

exhibit strong teleconnections (Figure S14 in Supporting Information S1). Further analysis using model runs with nudged SSTA could therefore allow disentangling the role of the central and Eastern Pacific on teleconnections to the Northern Pacific and North America.

The IO has a large number of most negatively curved links during EP conditions but not for CP (Figures 3c and 3d). The EP event teleconnections link the IO to the tropical Atlantic and Pacific basins (Figure 4c). The links to the tropical Atlantic could be either attributed to indirect links mediated by the impact of the Ninõ 3 region on the tropical Atlantic or might resemble direct impact between the oceans as recently described by L. Zhang and Han (2021). CP conditions do not result in teleconnections in the IO as CP events are generally weaker (W. Zhang et al., 2015).

The Labrador Sea (Figure 4d) is another pronounced area of most negative node-curvature in the CP network not present in the EP network (compare Figure 3c and 3d. Edges with the most negative curvature adjacent to the Labrador Sea connect to the extra topical Atlantic and, in contrast to Normal year conditions (Figure S13 in Supporting Information S1), to the Eastern Tropical Pacific. This pattern may be attributed to the North Atlantic Oscillation (NAO), which refers to sea level pressure changes in the Arctic and subtropical Atlantic (Jiménez-Esteve & Domeisen, 2018). El Niño is known to cause a negative NAO pattern driven by the PNA pattern where a negative NAO phase is attributable to CP El Niño events via the subtropical bridge (Domeisen et al., 2019; Graf & Zanchettin, 2012).

Note that we can identify the teleconnection patterns primarily because we have the results from the curvature-based climate network analysis to identify differences in the teleconnection structure and to guide our interpretations. Without the curvature analysis, for instance using classical complex network measures like betweenness centrality (Figure S7 in Supporting Information S1), it is not trivial to figure out the most important regions for each El Niño flavor.

4. Conclusion

We presented a new approach to estimate global teleconnection patterns of surface air temperature and used it to investigate the teleconnections of Eastern Pacific and Central Pacific El Niño events. Our approach involves the combination of correlation-based climate networks with a recently established network measure based on Ricci-curvature. In particular, we used Forman-Ricci curvature to distinguish links related to small-scale regional structures (positively curved links) from long-range teleconnections connecting regions from different parts of the globe (negatively curved links).

We showed that El Niño diversity drastically impacts the spatial organization of teleconnections. We identified teleconnection hotspots for both EP and CP conditions and showed that EP conditions strongly alternate the teleconnection structure of the climate network to be mainly confined to the tropics, whereas CP network teleconnections were found in northern and southern mid-latitudes as well. A comparison of the results from the application of our approach on SAT from the UKESM-LL2 Model from the CMIP6 project further corroborates our findings.

We further investigated the impact of ENSO diversity on the teleconnection patterns of four specific regions: the Niño 3 region, the Niño 4 region, the northern IO, and the Labrador Sea. We found that the Niño 3 region in the Eastern Pacific has a large number of teleconnections irrespective of whether we consider EP or CP conditions. The Niño 4 region in the Central Pacific has, in comparison, very few teleconnections under both EP and CP conditions and our analysis suggests that this is likely due to the higher spatio-temporal variability of anomalous SSTs in the Central Pacific. We conclude that the Eastern Pacific is the primary mediator of El Niño impacts irrespective of the El Niño type, and acknowledge that further work on the role of the Eastern Pacific during CP El Niños is needed.

We found that the northern IO and the Labrador Sea show teleconnections almost only under EP and CP conditions respectively. While the teleconnections of the IO region to the Niño 3 region during EP conditions are well-known, the links between the Labrador Sea to the Eastern Tropical Pacific and northern tropical Atlantic are not fully understood.

Data Availability Statement

Data sets for this research are available from Copernicus Climate Change Service. The data from 1959 till date was taken from Hersbach et al. (2018). The code for generating and analyzing the networks is made publicly available under Strnad and Schlör (2022). The code for reproducing the analysis of the network curvature described in this paper is publicly available under Schlör and Strnad (2022).

Acknowledgments
The authors would like to thank the reviewers for their helpful comments and suggestions. The authors acknowledge funding by the Deutsche Forschungsgemeinschaft (DFG, German Research Foundation) under Germany's Excellence Strategy—EXC number 2064/1—Project number 390727645. The authors thank the International Max Planck Research School for Intelligent Systems (IMPRS-IS) for supporting Jakob Schlör and Felix Strnad. Open Access funding enabled and organized by Projekt DEAL.

References

Alexander, M. A., Bladé, I., Newman, M., Lanzante, J. R., Lau, N.-C., & Scott, J. D. (2002). The atmospheric bridge: The influence of ENSO teleconnections on air–sea interaction over the Global Oceans. *Journal of Climate*, *15*(16), 2205–2231. https://doi.org/10.1175/1520-0442(2002)015<2205:TABTIO>2.0.CO;2

Amaya, D. J. (2019). The Pacific Meridional Mode and ENSO: A review. *Current Climate Change Reports*, *5*(4), 296–307. https://doi.org/10.1007/s40641-019-00142-x

Ashok, K., Behera, S. K., Rao, S. A., Weng, H., & Yamagata, T. (2007). El Niño Modoki and its possible teleconnection. *Journal of Geophysical Research*, *112*(C11), C11007. https://doi.org/10.1029/2006JC003798

Barsugli, J. J., & Sardeshmukh, P. D. (2002). Global atmospheric sensitivity to tropical SST anomalies throughout the Indo-Pacific basin. *Journal of Climate*, *15*(23), 3427–3442. https://doi.org/10.1175/1520-0442(2002)015<3427:GASTTS>2.0.CO;2

Bendito, E., Carmona, A., Encinas, A. M., & Gesto, J. M. (2007). Estimation of Fekete points. *Journal of Computational Physics*, *225*(2), 2354–2376. https://doi.org/10.1016/j.jcp.2007.03.017

Capotondi, A., & Ricciardulli, L. (2021). The influence of pacific winds on ENSO diversity. *Scientific Reports*, *11*(18672), 1–11. https://doi.org/10.1038/s41598-021-97963-4

Capotondi, A., Sardeshmukh, P. D., Di Lorenzo, E., Subramanian, A. C., & Miller, A. J. (2019). Predictability of US West Coast ocean temperatures is not solely due to ENSO. *Scientific Reports*, *9*(10993), 1–10. https://doi.org/10.1038/s41598-019-47400-4

Capotondi, A., Wittenberg, A., & Masina, S. (2006). Spatial and temporal structure of Tropical Pacific interannual variability in 20th century coupled simulations. *Ocean Modelling*, *15*(3), 274–298. https://doi.org/10.1016/j.ocemod.2006.02.004

Capotondi, A., Wittenberg, A. T., Kug, J.-S., Takahashi, K., & McPhaden, M. J. (2020). ENSO diversity. In *El Niño Southern Oscillation in a changing climate* (pp. 65–86). American Geophysical Union (AGU). https://doi.org/10.1002/9781119548164.ch4

Capotondi, A., Wittenberg, A. T., Newman, M., Di Lorenzo, E., Yu, J.-Y., Braconnot, P., et al. (2015). Understanding ENSO diversity. *Bulletin of the American Meteorological Society*, *96*(6), 921–938. https://doi.org/10.1175/BAMS-D-13-00117.1

Chang, P., Fang, Y., Saravanan, R., Ji, L., & Seidel, H. (2006). The cause of the fragile relationship between the Pacific El Niño and the Atlantic Niño. *Nature*, *443*(7109), 324–328. https://doi.org/10.1038/nature05053

Chen, M., Yu, J.-Y., Wang, X., & Chen, S. (2021). Distinct onset mechanisms of two subtypes of CP El Niño and their changes in future warming. *Geophysical Research Letters*, *48*(14), e2021GL093707. https://doi.org/10.1029/2021GL093707

de Souza, D. B., da Cunha, J. T. S., dos Santos, E. F., Correia, J. B., da Silva, H. P., de Lima Filho, J. L., et al. (2021). Using discrete Ricci curvatures to infer COVID-19 epidemic network fragility and systemic risk. *Journal of Statistical Mechanics: Theory and Experiment*, *2021*(5), 053501. https://doi.org/10.1088/1742-5468/abed4e

Dieppois, B., Capotondi, A., Pohl, B., Chun, K. P., Monerie, P.-A., & Eden, J. (2021). ENSO diversity shows robust decadal variations that must be captured for accurate future projections. *Communications Earth & Environment*, *2*(212), 1–13. https://doi.org/10.1038/s43247-021-00285-6

Dijkstra, H. A., Hernández-García, E., Masoller, C., & Barreiro, M. (2019). Networks in climate. https://doi.org/10.1017/9781316275757

Domeisen, D. I. V., Garfinkel, C. I., & Butler, A. H. (2019). The teleconnection of El Niño Southern Oscillation to the stratosphere. *Review of Geophysics*, *57*(1), 5–47. https://doi.org/10.1029/2018RG000596

Donges, J. F., Zou, Y., Marwan, N., & Kurths, J. (2009). Complex networks in climate dynamics. *The European Physical Journal—Special Topics*, *174*(1), 157–179. https://doi.org/10.1140/epjst/e2009-01098-2

Ebert-Uphoff, I., & Deng, Y. (2012). A new type of climate network based on probabilistic graphical models: Results of boreal winter versus summer. *Geophysical Research Letters*, *39*(18), 1–7. https://doi.org/10.1029/2012GL053269

Eyring, V., Bony, S., Meehl, G. A., Senior, C. A., Stevens, B., Stouffer, R. J., & Taylor, K. E. (2016). Overview of the Coupled Model Intercomparison Project Phase 6 (CMIP6) experimental design and organization. *Geoscientific Model Development*, *9*(5), 1937–1958. https://doi.org/10.5194/gmd-9-1937-2016

Farooq, H., Chen, Y., Georgiou, T. T., Tannenbaum, A., & Lenglet, C. (2019). Network curvature as a hallmark of brain structural connectivity. *Nature Communications*, *10*(4937), 1–11. https://doi.org/10.1038/s41467-019-12915-x

Forman, R. (2003). Bochner's method for cell complexes and combinatorial Ricci curvature. *Discrete & Computational Geometry*, *29*(3), 323–374. https://doi.org/10.1007/s00454-002-0743-x

Gao, L., Liu, X., Liu, Y., Wang, P., Deng, M., Zhu, Q., & Li, H. (2019). Measuring road network topology vulnerability by Ricci curvature. *Physica A*, *527*, 121071. https://doi.org/10.1016/j.physa.2019.121071

Graf, H.-F., & Zanchettin, D. (2012). Central Pacific El Niño, the "subtropical bridge," and Eurasian climate. *Journal of Geophysical Research*, *117*(D1), 1102. https://doi.org/10.1029/2011JD016493

Ham, Y.-G., & Kug, J.-S. (2012). How well do current climate models simulate two types of El Nino? *Climate Dynamics*, *39*(1), 383–398. https://doi.org/10.1007/s00382-011-1157-3

Hersbach, H., Bell, B., Berrisford, P., Biavati, G., Horányi, A., Muñoz Sabater, J., et al. (2018). Era5 hourly data on single levels from 1979 to present. Copernicus climate change Service (C3S) climate data Store (CDS). https://doi.org/10.24381/cds.adbb2d47

Hersbach, H., Bell, B., Berrisford, P., Hirahara, S., Horányi, A., Muñoz-Sabater, J., et al. (2020). The ERA5 global reanalysis. *Quarterly Journal of the Royal Meteorological Society*, *146*(730), 1999–2049. https://doi.org/10.1002/qj.3803

Huang, B. (2004). Remotely forced variability in the Tropical Atlantic Ocean. *Climate Dynamics*, *23*(2), 133–152. https://doi.org/10.1007/s00382-004-0443-8

Jiménez-Esteve, B., & Domeisen, D. I. V. (2018). The tropospheric pathway of the ENSO–North Atlantic teleconnection. *Journal of Climate*, *31*(11), 4563–4584. https://doi.org/10.1175/JCLI-D-17-0716.1

Johnson, N. C. (2013). How many ENSO flavors can we distinguish? *Journal of Climate*, *26*(13), 4816–4827. https://doi.org/10.1175/JCLI-D-12-00649.1

Jonckheere, E., & Grippo, E. (2019). Ollivier-Ricci curvature approach to cost-effective power grid congestion management. In *2019 Chinese control and decision conference (CCDC)* (pp. 2118–2123). IEEE. https://doi.org/10.1109/CCDC.2019.8832819

Kao, H.-Y., & Yu, J.-Y. (2009). Contrasting eastern-Pacific and Central-Pacific types of ENSO. *Journal of Climate*, *22*(3), 615–632. https://doi.org/10.1175/2008JCLI2309.1

Kittel, T., Ciemer, C., Lotfi, N., Peron, T., Rodrigues, F., Kurths, J., & Donner, R. V. (2021). Evolving climate network perspectives on global surface air temperature effects of ENSO and strong volcanic eruptions. *The European Physical Journal—Special Topics*, *230*(14), 3075–3100. https://doi.org/10.1140/epjs/s11734-021-00269-9

Klein, S. A., Soden, B. J., & Lau, N.-C. (1999). Remote sea surface temperature variations during ENSO: Evidence for a tropical atmospheric bridge. *Journal of Climate*, *12*(4), 917–932. https://doi.org/10.1175/1520-0442(1999)012<0917:RSSTVD>2.0.CO;2

Kug, J.-S., Choi, J., An, S.-I., Jin, F.-F., & Wittenberg, A. T. (2010). Warm pool and cold tongue El Niño events as simulated by the GFDL 2.1 coupled GCM. *Journal of Climate*, *23*(5), 1226–1239. https://doi.org/10.1175/2009JCLI3293.1

Lambert, F. H., Webb, M. J., & Joshi, M. M. (2011). The relationship between land–ocean surface temperature contrast and radiative forcing. *Journal of Climate*, *24*(13), 3239–3256. https://doi.org/10.1175/2011JCLI3893.1

Lu, Z., Yuan, N., Chen, L., & Gong, Z. (2020). On the impacts of El Niño events: A new monitoring approach using complex network analysis. *Geophysical Research Letters*, *47*(6), e2019GL086533. https://doi.org/10.1029/2019GL086533

Okumura, Y. M. (2019). ENSO diversity from an atmospheric perspective. *Current Climate Change Reports*, *5*(3), 245–257. https://doi.org/10.1007/s40641-019-00138-7

Ollivier, Y. (2009). Ricci curvature of Markov chains on metric spaces. *Journal of Functional Analysis*, *256*(3), 810–864. https://doi.org/10.1016/j.jfa.2008.11.001

Ollivier, Y. (2010). A survey of Ricci curvature for metric spaces and Markov chains. In *Probabilistic approach to geometry* (pp. 343–381). Mathematical Society of Japan.

Pouryahya, M., Oh, J. H., Mathews, J. C., Deasy, J. O., & Tannenbaum, A. R. (2018). Characterizing cancer drug response and biological correlates: A geometric network approach. *Scientific Reports*, *8*(6402), 1–12. https://doi.org/10.1038/s41598-018-24679-3

Radebach, A., Donner, R. V., Runge, J., Donges, J. F., & Kurths, J. (2013). Disentangling different types of El Niño episodes by evolving climate network analysis. *Physical Review E—Statistical Physics, Plasmas, Fluids, and Related Interdisciplinary Topics*, *88*(5), 052807. https://doi.org/10.1103/PhysRevE.88.052807

Rasmusson, E. M., & Carpenter, T. H. (1982). Variations in tropical sea surface temperature and surface wind fields associated with the Southern Oscillation/El Niño. *Monthly Weather Review*, *110*(5), 354–384. https://doi.org/10.1175/1520-0493(1982)110<0354:vitsst>2.0.co;2

Rodrigues, R. R., Campos, E. J. D., & Haarsma, R. (2015). The impact of ENSO on the South Atlantic subtropical dipole mode. *Journal of Climate*, *28*(7), 2691–2705. https://doi.org/10.1175/JCLI-D-14-00483.1

Rodrigues, R. R., Haarsma, R. J., Campos, E. J. D., & Ambrizzi, T. (2011). The impacts of Inter–El Niño variability on the Tropical Atlantic and Northeast Brazil climate. *Journal of Climate*, *24*(13), 3402–3422. https://doi.org/10.1175/2011JCLI3983.1

Samal, A., Sreejith, R. P., Gu, J., Liu, S., Saucan, E., & Jost, J. (2018). Comparative analysis of two discretizations of Ricci curvature for complex networks. *Scientific Reports*, *8*(8650), 1–16. https://doi.org/10.1038/s41598-018-27001-3

Sandhu, R., Georgiou, T., Reznik, E., Zhu, L., Kolesov, I., Senbabaoglu, Y., & Tannenbaum, A. (2015). Graph curvature for differentiating cancer networks. *Scientific Reports*, *5*(12323), 1–13. https://doi.org/10.1038/srep12323

Sandhu, R. S., Georgiou, T. T., & Tannenbaum, A. R. (2016). Ricci curvature: An economic indicator for market fragility and systemic risk. *Science Advances*, *2*(5). https://doi.org/10.1126/sciadv.1501495%23F2

Schlör, J., & Strnad, F. (2022). Netcurvature. *Zenodo*. https://doi.org/10.5281/zenodo.6325299

Shi, J., Fedorov, A. V., & Hu, S. (2019). North Pacific temperature and precipitation response to El Niño-like equatorial heating: Sensitivity to forcing location. *Climate Dynamics*, *53*(5), 2731–2741. https://doi.org/10.1007/s00382-019-04655-x

Sreejith, R., Mohanraj, K., Jost, J., Saucan, E., & Samal, A. (2016). Forman curvature for complex networks. *Journal of Statistical Mechanics: Theory and Experiment*, *2016*(6), 063206. https://doi.org/10.1088/1742-5468/2016/06/063206

Strnad, F., & Schlör, J. (2022). Climnet. *Zenodo*. https://doi.org/10.5281/zenodo.6325661

Taschetto, A. S., Ummenhofer, C. C., Stuecker, M. F., Dommenget, D., Ashok, K., Rodrigues, R. R., & Yeh, S.-W. (2020). ENSO atmospheric teleconnections. In *El Niño Southern Oscillation in a changing climate* (pp. 309–335). American Geophysical Union (AGU). https://doi.org/10.1002/9781119548164.ch14

Timmermann, A., An, S.-I., Kug, J.-S., Jin, F.-F., Cai, W., Capotondi, A., et al. (2018). El Niño–Southern Oscillation complexity. *Nature*, *559*(7715), 535–545. https://doi.org/10.1038/s41586-018-0252-6

Trenberth, K. E. (1997). The definition of El Niño. *Bulletin of the American Meteorological Society*, *78*(12), 2771–2778. https://doi.org/10.1175/1520-0477(1997)078<2771:tdoeno>2.0.co;2

Trenberth, K. E., & Stepaniak, D. P. (2001). Indices of El Niño Evolution. *Journal of Climate*, *14*(8), 1697–1701. https://doi.org/10.1175/1520-0442(2001)014<1697:lioeno>2.0.co;2

Tsonis, A. A., & Swanson, K. L. (2008). Topology and predictability of El Niño and La Niña networks. *Physical Review Letters*, *100*(22), 228502. https://doi.org/10.1103/PhysRevLett.100.228502

Wang, C., & Wang, X. (2013). Classifying El Niño Modoki I and II by different impacts on rainfall in Southern China and typhoon tracks. *Journal of Climate*, *26*(4), 1322–1338. https://doi.org/10.1175/JCLI-D-12-00107.1

Wang, G., & Hendon, H. H. (2007). Sensitivity of Australian rainfall to Inter–El Niño variations. *Journal of Climate*, *20*(16), 4211–4226. https://doi.org/10.1175/JCLI4228.1

Wang, X., & Wang, C. (2014). Different impacts of various El Niño events on the Indian Ocean dipole. *Climate Dynamics*, *42*(3), 991–1005. https://doi.org/10.1007/s00382-013-1711-2

Wiedermann, M., Radebach, A., Donges, J. F., Kurths, J., & Donner, R. V. (2016). A climate network-based index to discriminate different types of El Niño and La Niña. *Geophysical Research Letters*, *43*(13), 7176–7185. https://doi.org/10.1002/2016GL069119

Yamasaki, K., Gozolchiani, A., & Havlin, S. (2008). Climate networks around the globe are significantly affected by El Niño. *Physical Review Letters*, *100*(22), 228501. https://doi.org/10.1103/PhysRevLett.100.228501

You, Y., & Furtado, J. C. (2018). The South Pacific Meridional Mode and its role in tropical Pacific climate variability. *Journal of Climate*, *31*(24), 10141–10163. https://doi.org/10.1175/JCLI-D-17-0860.1

Yu, J.-Y., Zou, Y., Kim, S. T., & Lee, T. (2012). The changing impact of El Niño on US winter temperatures. *Geophysical Research Letters*, *39*(15). https://doi.org/10.1029/2012GL052483

Zhang, L., & Han, W. (2021). Indian Ocean dipole leads to Atlantic Niño. *Nature Communications*, *12*(5952), 1–9. https://doi.org/10.1038/s41467-021-26223-w

Zhang, W., Wang, Y., Jin, F.-F., Stuecker, M. F., & Turner, A. G. (2015). Impact of different El Niño types on the El Niño/IOD relationship. *Geophysical Research Letters*, *42*(20), 8570–8576. https://doi.org/10.1002/2015GL065703

Zhou, D., Gozolchiani, A., Ashkenazy, Y., & Havlin, S. (2015). Teleconnection paths via climate network direct link detection. *Physical Review Letters*, *115*(26), 268501. https://doi.org/10.1103/PhysRevLett.115.268501